Available online at www.sciencedirect.com
SCIENCE DIRECT®
Sensors and Actuators A 122 (2005) 307–316
SENSORS AND ACTUATORS A PHYSICAL
www.elsevier.com/locate/sna

Electrically coupled MEMS bandpass filters Part I: With coupling element

Siavash Pourkamali, Farrokh Ayazi *

School of Electrical and Computer Engineering, Georgia Institute of Technology, 791 Atlantic Drive, Atlanta, GA 30332-0250, USA

Received 30 April 2004; accepted 9 March 2005
Available online 3 May 2005

Abstract

This paper, the first of the two parts, presents coupling techniques for implementation of high order narrow-bandwidth bandpass filters from micromechanical resonators using electrical coupling elements. Active and passive coupling elements are used in this work to implement high order resonant systems from individual MEMS resonators. The concept of passive coupling of resonators using capacitors as the coupling elements for filter synthesis and its electromechanical modeling is presented. Active coupling of resonators using transistor-based amplifying circuits is introduced and demonstrated as well. Capacitively coupled bandpass filters with integrated coupling capacitors and filter quality factor as high as 1500 at operating frequency of 810 kHz are practically demonstrated. 2× *Q*-amplification was obtained from a resonator array consisting of three resonator stages interconnected with active interface circuits.

Keywords: Micromechanical filter; Microresonator; Coupling; HARPSS; Quality factor

1. Introduction

Silicon-based MEMS resonators with their high quality factors, low cost batch fabrication, small size and IC compatibility have a great potential as frequency selective components (i.e. frequency references and filters) in modern, highly integrated electronic systems. Extensive research is currently underway to replace off-chip macro-scale resonant devices in such systems with on-chip silicon-micromachined MEMS resonators. Despite high quality factors in the order of tens of thousands, a single resonator is a first-order resonant system providing limited frequency selectivity. When used as bandpass filters, in order to provide higher selectivity, higher order resonant systems comprising of a number of coupled resonators are required.

Mechanical coupling techniques, traditionally used for implementation of higher order filters from macro-scale mechanical resonators [1], have been applied to micromechanical resonators [2–6]. Electrically sensed and actuated MEMS filters up to the third-order [2] and center frequencies up to 68 MHz [3] as well as electrically actuated and optically sensed filters up to the 20th-order at center frequencies of a few megahertz [5] have been demonstrated using the mechanical coupling approach. As the size of the micromechanical resonators is reduced to reach higher operating frequencies in the VHF and UHF range, to avoid mass loading of the resonators by the coupling elements and have a reasonably narrow filter bandwidth, mechanical coupling of resonators may require very small coupling elements (e.g., submicron in width wires) that are difficult to implement reproducibly using low cost manufacturing processes. In addition, the characteristics of mechanically coupled filters (i.e. bandwidth) are determined solely by the physical dimensions of the filter and can fairly be tuned to the required values after fabrication [6].

This work presents electrical-based coupling techniques for implementation of higher order bandpass filters from individual micromechanical resonators. Different variations of electrical coupling are introduced. Two different electrical coupling techniques utilizing electrical coupling elements [7] are discussed and demonstrated in this part: (1) capacitive

* Corresponding author. Tel.: +1 404 894 9496; fax: +1 404 385 6650.
E-mail addresses: siavash@ece.gatech.edu (S. Pourkamali), ayazi@ece.gatech.edu (F. Ayazi).

0924-4247/$ – see front matter © 2005 Elsevier B.V. All rights reserved.
doi:10.1016/j.sna.2005.03.038

coupling (passive) and (2) active cascading of resonators. Electrical coupling without the need for physical coupling elements is presented in part II of this paper. In the passive coupling approach, capacitors are used to couple MEMS resonators to each other and provide a higher order bandpass transfer function. Amplifying interface circuits in between the resonators are used as the coupling elements for active coupling of resonators.

The main advantage of electrical coupling approaches for filter synthesis is their greater potential for extension of the frequency into the UHF range. Filter synthesis using electrical coupling does not require mechanical design expertise and provides more design flexibility for electrical engineers. In addition, electrically coupled micromechanical filters have superior tunability compared to their mechanically coupled counterparts and can be biased to the desired characteristics after fabrication.

High-Q single crystal silicon (SCS) capacitive resonators [8–10] with operating frequencies in the medium frequency band (300 kHz–3 MHz) are used as building blocks of passive and active electrically coupled MEMS bandpass filters.

2. Capacitive coupling

Fig. 1 shows the equivalent circuit model of a two-port capacitive micromechanical resonator. The *RLC* series tank represents the mechanical nature of the resonating element that is comprised of mass (M), stiffness (K) and loss elements providing a second-order bandpass transfer function with a pair of conjugate poles at its resonance frequency. As given by Eq. (1), the equivalent motional resistance of the device is determined by the area of the sense and drive electrodes (A_e), the capacitive gap size between the electrodes and the resonator (d), the applied dc polarization voltage (V_p) and the mechanical quality factor (Q) of the resonator. ε_0 is the permitivity coefficient of vacuum.

$$R_m = \frac{\sqrt{KM}d^4}{Q\varepsilon_0^2 A_e^2 V_p^2} \tag{1}$$

The input and output terminating capacitors represent the physical capacitors that are present at the input and output nodes of the resonator. Such capacitors include the capacitance between the electrodes and the resonating body as well as any wire-bonding pad or parasitic capacitor associated with the device. The transformers at the terminations of the device (Fig. 1) count for any asymmetry between the sense and drive electrodes that results in different input and output impedance levels. For a symmetric resonator, the transformers in the electrical model have a transformation ratio of unity; therefore, the equivalent circuit will be reduced to a series *RLC* tank terminated by two capacitors at the input and output.

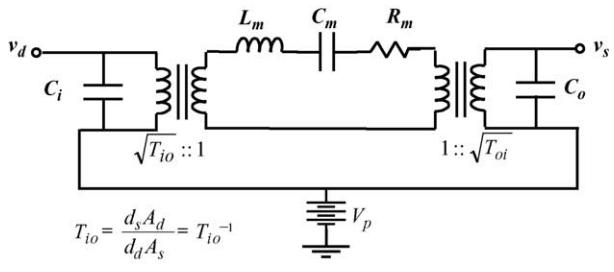

Fig. 1. Electrical equivalent circuit of a two-port capacitive MEMS resonator: d_d, d_s, A_d and A_s are drive and sense electrode capacitive gaps and effective area, respectively.

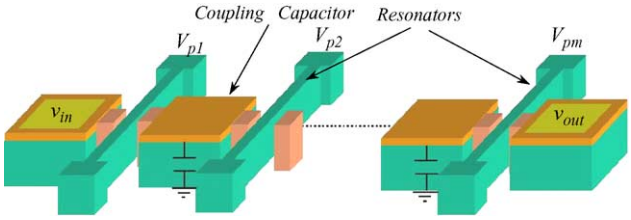

Fig. 2. Schematic diagram of a capacitively coupled microelectromechanical filter array.

In the capacitive coupling approach, as depicted in Fig. 2, micromechanical resonators are cascaded with shunt capacitors to ground in between every two adjacent resonators. The coupling capacitors interact with the equivalent *RLC* tanks of the resonators resulting in several resonance modes for the system and consequently a multiple order bandpass frequency response.

2.1. Filter operation

Assume a two-resonator (second-order) capacitively coupled resonant system, consisting of a coupling capacitor and two similar resonators with center frequency (f_0), quality factors ($Q > 1000$) and motional resistances (R_m). Insertion of the shunt coupling capacitor in between the two resonators results in a new pair of conjugate poles in the transfer function of the system at the frequency given by Eq. (2).

$$f_1 = f_0\sqrt{\frac{1 + \pi f_0 C_c R Q}{\pi f_0 C_c R Q}} \tag{2}$$

This will introduce a new resonance mode for the system in addition to the inherent resonance mode of the individual resonators at f_0. Fig. 3 shows the electrical equivalent circuit and frequency response of a second-order capacitively coupled resonant system showing how the extra resonance mode is created. For simplicity, the resonators are assumed to be symmetric and the corresponding input and output capacitances are neglected. Looking at the frequency response of the two-resonator system, the first resonance occurs at the mechanical resonant frequency of the individual resonators. At the first resonance, as shown in Fig. 3, the two resonators resonate in phase and the coupling capacitor has negligible contribution (while C_c is being charged by the first resonator, the other resonator is discharging it). At the second resonance mode (f_1), however, the two resonators vibrate with a 180°

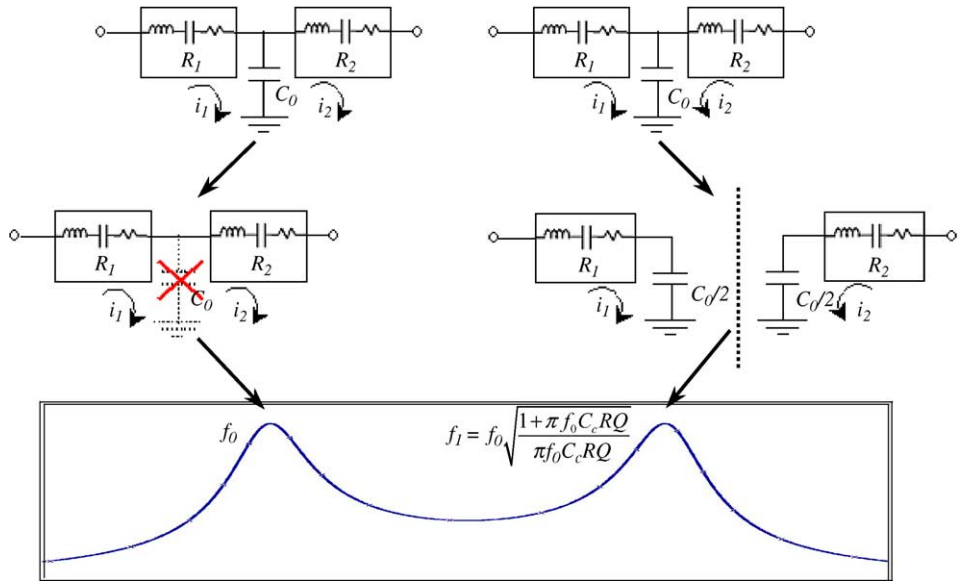

Fig. 3. Electrical schematic diagram of a second-order capacitively coupled resonant system and its frequency response.

phase difference and hence the coupling capacitor comes into the game (it is being charged and discharged at the same time by both resonators). Due to symmetry in this resonance mode, the system can be split into two equivalent half circuits each consisting of one resonator and a series capacitor $C_c/2$ to ground. The coupling capacitor in series with the motional capacitance of the resonator (C_m) reduces the total capacitance of the *RLC* tank, causing the second resonance mode to have a higher frequency as given by Eq. (2).

Fig. 4 shows the electrical equivalent circuit and frequency response for a third-order capacitively coupled resonant array. For the third-order system, in the first resonance mode, all resonators resonate in phase canceling the effect of coupling capacitors. In the second resonance mode, the two

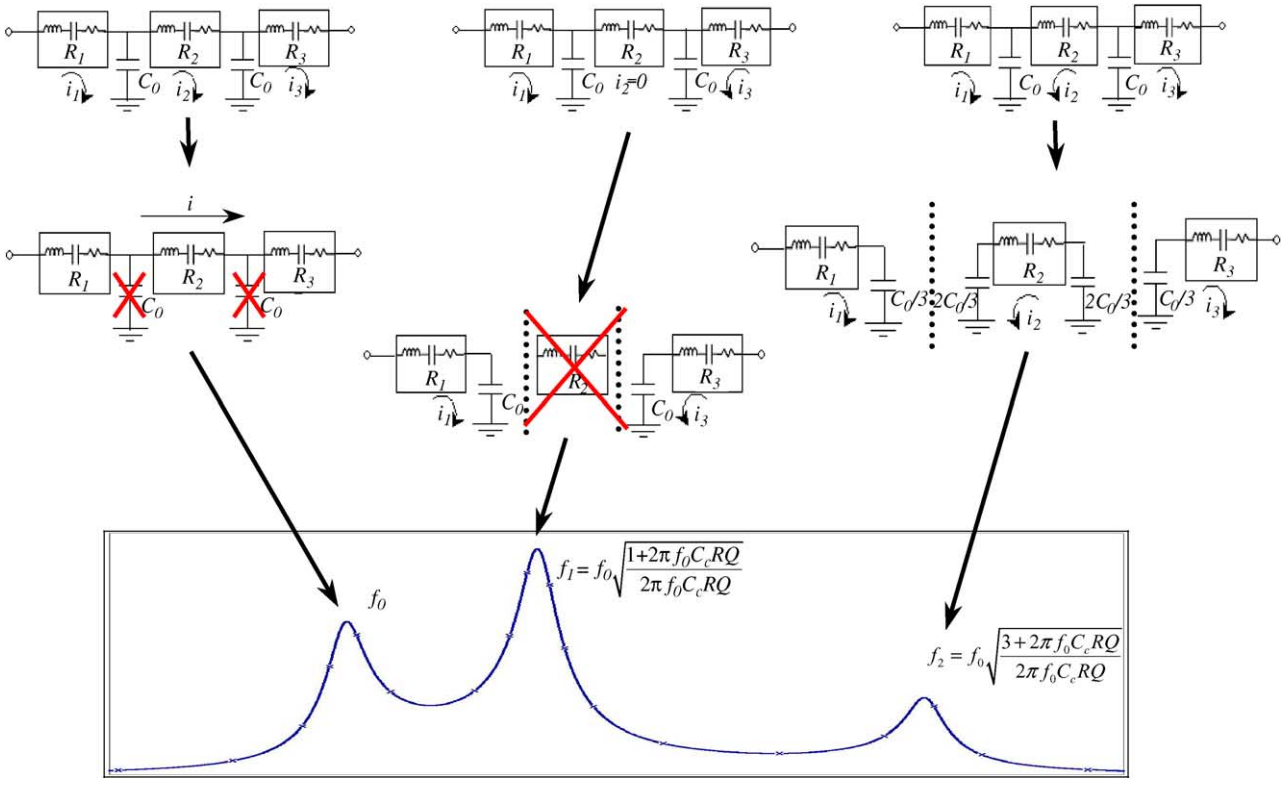

Fig. 4. Electrical schematic diagram of a third-order capacitively coupled resonant system and its frequency response.

terminating resonators resonate with a 180° phase difference and due to symmetry, no current passes through the resonator in the middle (Fig. 4). Therefore, each of the terminating resonators will be in series with a coupling capacitor, resulting in a higher frequency resonance mode at:

$$f_1 = f_0\sqrt{\frac{1+2\pi f_0 C_c R Q}{2\pi f_0 C_c R Q}}. \quad (3)$$

In the third resonance mode, all the adjacent resonators resonate out of phase (180° phase difference) with respect to each other. The coupling capacitors in this mode are split between the resonators so that they result in the same resonance frequency for all of them (one-third of a capacitor for each terminating resonator and two-third of each capacitor for the middle resonator). The resulting frequency is:

$$f_2 = f_0\sqrt{\frac{3+2\pi f_0 C_c R Q}{2\pi f_0 C_c R Q}}. \quad (4)$$

The asymmetry in the frequency response of the third-order filter is due to the fact that the terminating resonators have only one coupling capacitor next to them but the one in the middle is terminated with two coupling capacitors. This asymmetry that also happens for higher order arrays can be compensated by slight frequency tuning of the terminating resonators of the chain with respect to the rest of the resonators. On the other hand, for optimum operation of the filter, it is necessary that all resonators in the chain have equal center frequencies and the slight frequency mismatch results in an increased insertion loss. The more efficient solution to this problem is to use a closed chain of coupled resonators [5] providing complete symmetry for all the resonators.

2.2. Insertion loss

The insertion loss of a capacitively coupled filter (assuming ideal lossless coupling capacitors) is determined by the order of the filter, the equivalent motional resistance of the resonators and the terminating resistor values that flatten the filter passband. In a real case, when the filter is incorporated in an electrical system, the terminating resistors are the input and output equivalent resistance of the electronic stages adjacent to the filter (i.e. low noise amplifiers). With good approximation, an *n*th order filter at resonance is equivalent to *n* resistors, each having value of R_m, in series. Therefore,

$$\text{insertion loss(dB)} = 20\log\left(\frac{nR_m + 2R_{term}}{2R_{term}}\right) \quad (5)$$

where R_{term} is the terminating resistor value. The required terminating resistance value depends on filter bandwidth, maximum tolerable passband ripple and motional resistance of the resonators. For a specific value of coupling capacitor and resonators with similar design parameters (gap size, electrode area and polarization voltage) resulting in equal equivalent motional capacitance (C_m) and consequently equal filter bandwidths, the motional resistance is determined by the quality factor of the resonators. Therefore, filter insertion loss will depend on the quality factor of individual resonators. Fig. 5 illustrates simulation results of second- and third-order capacitively coupled electromechanical filters at 600 kHz with different resonator quality factors, showing dependence of filter insertion loss on the *Q* of individual resonators.

For the specific filter characteristics of Fig. 5, coupling capacitors of 0.15 and 0.2 pF are used that can be easily fabricated on-chip in any MEMS or CMOS process. According to Eqs. (2)–(4), the required coupling capacitor values are determined by the motional resistance of the resonators,

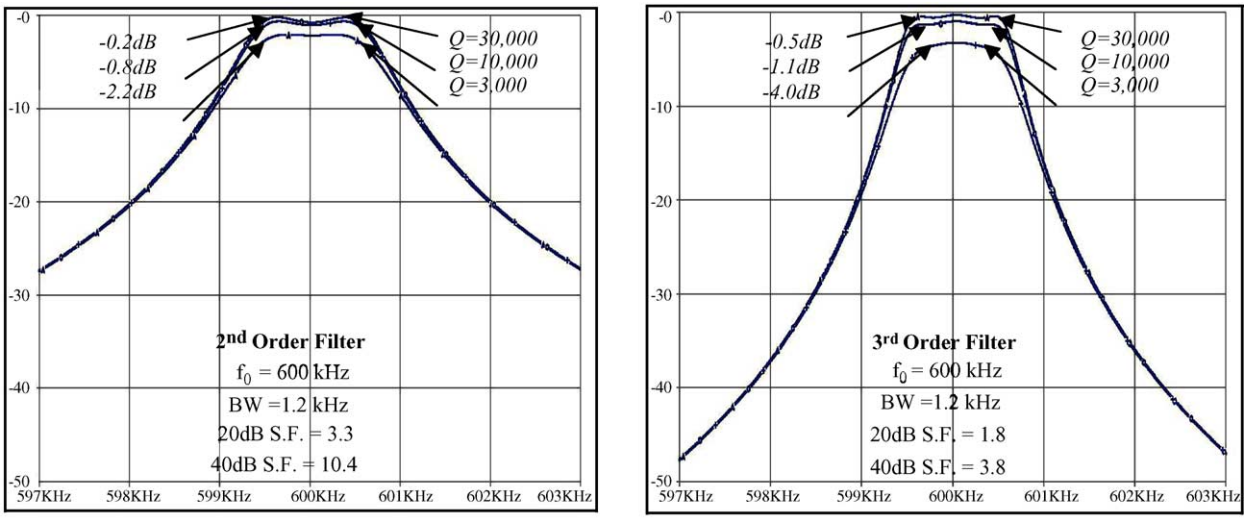

* S.F. = shape factor, and BW = bandwidth.

Fig. 5. Simulation results for 600 kHz capacitively coupled second- and third-order filters. A higher resonator *Q* results in a lower insertion loss. Coupling capicitance: $C_c = 0.15$ pF (second-order); $C_c = 0.2$ pF (third-order) and $R_{term} = 50$ kΩ. S.F.: shape factor and BW: bandwidth.

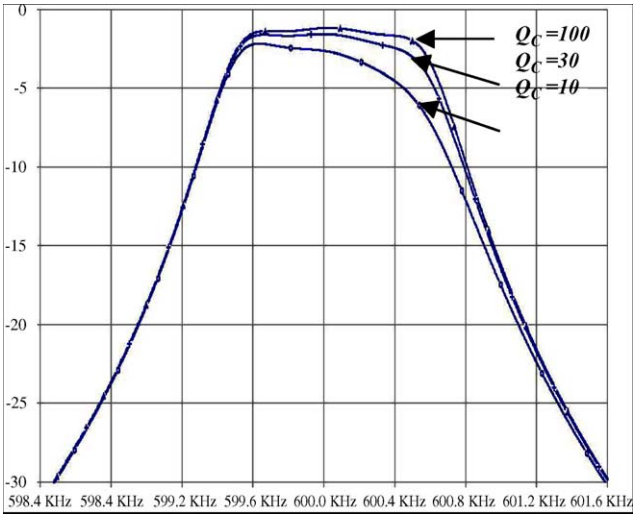

Fig. 6. Effect of finite Q of the coupling capacitors on the frequency response of a third-order capacitively coupled filter.

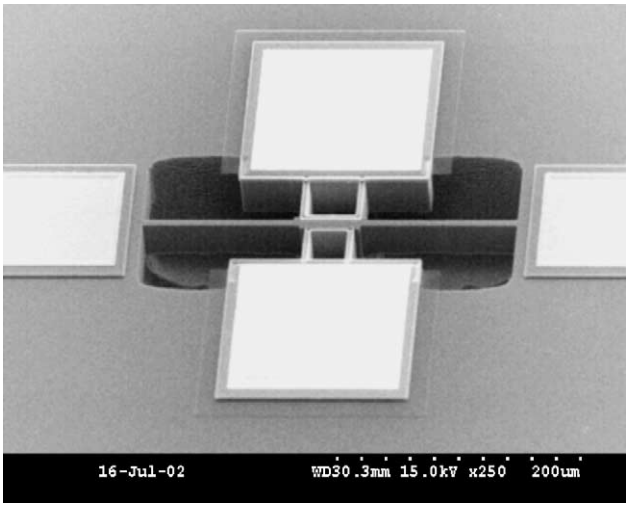

Fig. 7. 300 μm long, 7 μm wide and 25 μm thick HARPSS SCS beam resonator fabricated on a regular silicon substrate (f_0 = 600 kHz).

operating frequency, order of the filter and the desired filter bandwidth.

2.3. Loss in the coupling capacitors

Fig. 6 shows the simulated frequency response of the third-order capacitively coupled filter of Fig. 5 (resonator Q = 10,000) with non-ideal (lossy) coupling capacitors. Since the coupling capacitors do not have a significant role in the first resonance mode, their finite Q does not have a significant effect on the first resonance peak but its attenuation effect becomes more pronounced in higher resonance modes.

2.4. Implementation with off-chip interconnections

Single crystal silicon capacitive HARPSS resonators fabricated on regular silicon substrates [8] were used to demonstrate preliminary results for capacitively coupled bandpass filters. SEM view of a 600 kHz HARPSS SCS resonator is shown in Fig. 7. Such resonators are comprised of SCS in-plane resonating element and polysilicon sense and drive electrodes. The capacitive transduction gaps are defined in a self-aligned process step by the thickness of a sacrificial oxide layer and can be scaled down to tens of nanometer. The 600 kHz SCS clamped–clamped beam resonators used in this work have capacitive gap size of 700 nm and quality factor of ∼10,000.

In order to demonstrate a 600 kHz second-order filter, two HARPSS resonators on different silicon chips were mounted and wire-bonded on a PCB containing a low noise JFET-input amplifier to sense the output signal of the filter. The PCB was placed in a custom vacuum system which kept the pressure below 1 mTorr. The output of the first resonator was directly connected to the second resonator through wirebonds and the metal track on the PCB. The frequency response of the filter was measured using an Agilent 4395A network analyzer. Since the resonating body of HARPSS resonators fabricated on regular silicon substrates are electrically connected to the silicon substrate, the two resonators have to be on different substrates so that their resonance frequencies can be tuned independently by applying different polarization voltage values. The parasitic capacitances introduced by the wirebonds and the PCB in addition to the large pad capacitors of the resonators (∼1 pF) resulted in a total coupling capacitor of ∼3 pF. With such a large coupling capacitor, separation of the two resonance peaks is less than the bandwidth of individual resonators and two separate resonance peaks were not observed after tuning the frequencies (Fig. 8). However, the measured shape factor values confirm the second-order nature of the system. Fig. 9 shows simulation result of the measured

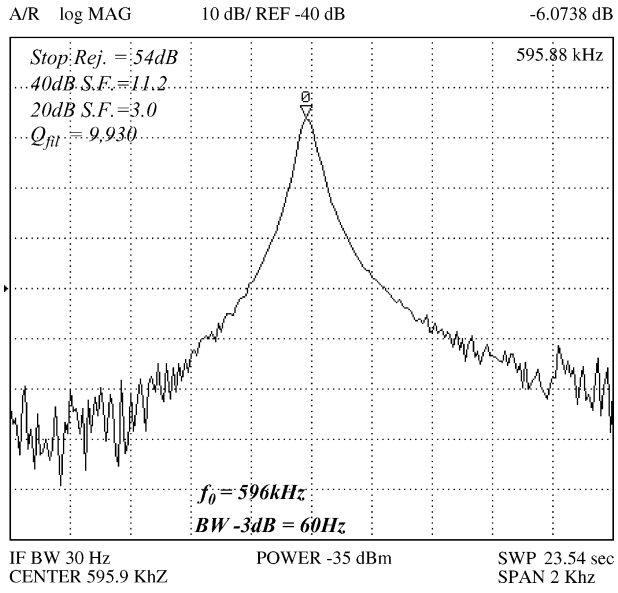

Fig. 8. Frequency response of a second-order capacitively coupled resonator array with off-chip interconnections.

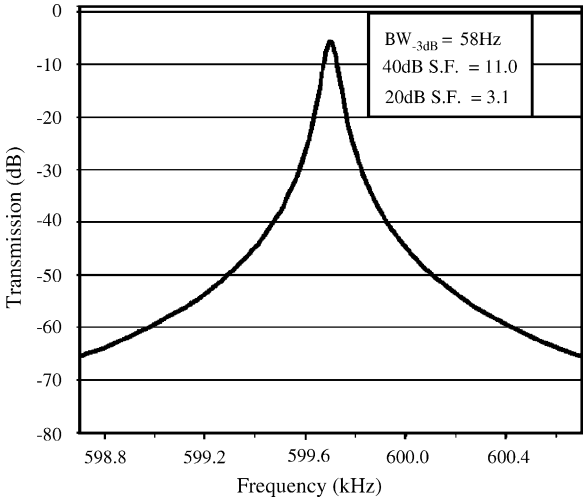

Fig. 9. Simulation results for coupled resonator array of Fig. 8 showing good agreement between the simulation and measurement.

filter with 3 pF parasitic coupling capacitance showing excellent agreement between the measurement and simulation.

2.5. Implementation with integrated coupling capacitor

To overcome the problems associated with off-chip interconnection and large parasitics, capacitively coupled filters with integrated coupling capacitors were fabricated on SOI substrates. SOI substrates provide the capability of electrical isolation between the resonators and, therefore, different resonators in the same filter array can be tuned independently. The resonators were fabricated using a self-aligned submicron trench etching technique [10] and are fully made of single crystal silicon. The width of the capacitive gaps in such devices is defined in a self-aligned manner by the thickness of a sacrificial polysilicon layer and can be reduced down to deep-submicron levels without the need for nanolithography. Deep-submicron capacitive gaps are then dry etched using the Bosch process in an inductively coupled plasma system (ICP). Fig. 10 shows the SEM view of a fabricated second-order capacitively coupled bandpass filter. The filter consists of two clamped–clamped beam resonators, each 178 μm long, 3.7 μm wide and 4.5 μm thick with 350 nm wide dry-etched capacitive transducer gaps. The quality factor of individual resonators was measured to be 5000 at resonance frequency of 800 kHz. The output electrode of the first resonator is connected to the input of the second resonator through a 50 μm wide and 155 μm long silicon island. The handle layer of the SOI substrate is connected to dc ground so that the capacitance between the interconnecting silicon island and the handle layer acts as the coupling capacitor. The thickness of the buried oxide layer of the SOI substrate for the device of Fig. 10 is 5 μm resulting in a 45 fF coupling capacitor value.

Fig. 11 shows the schematic diagram of the measurement setup for characterization of integrated capacitively coupled

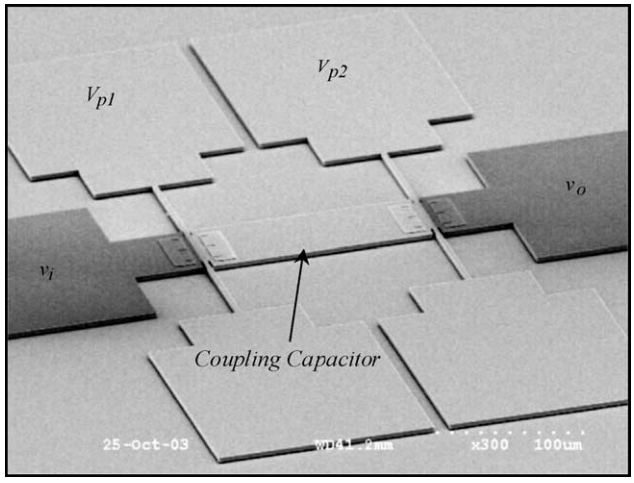

Fig. 10. SEM view of a second-order 800 kHz capacitively coupled filter with integrated coupling capacitor.

filters. The filters were tested under vacuum in a vacuum probe-station. Two different polarization voltages were applied to the two resonators in order to tune their center frequencies to equal values. One of the main concerns for measurement of such devices was dc biasing of the coupling capacitor. Since very small values of coupling capacitors in the order of tens of femto-Farads are required for proper operation of such filters, addition of any extra biasing elements to set a constant dc bias value for the coupling capacitor will cause a large overall capacitance at the coupling node and deteriorate filter characteristics [11]. In order to alleviate the biasing problem without adding extra biasing elements, polarization voltages with opposite polarities were applied to the two resonators causing the coupling capacitor to have a dc value equal to the average of the two polarization voltages which is close to zero. As a result, there will be enough dc voltage difference for signal transduction between each of the resonators and the coupling capacitor that also acts as the input and output electrode of the coupled resonators.

Fig. 12 shows the frequency response of the 800 kHz filter of Fig. 10 with different values of polarization voltages applied to the resonators. According to Eq. (2), as the equivalent resistance of the resonators decreases by increasing the

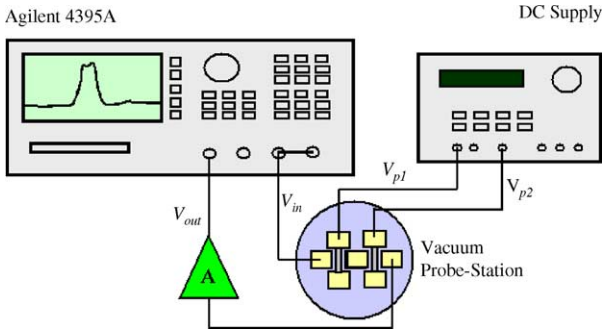

Fig. 11. Schematic of the test setup for measurement of arrays of capacitively coupled beam resonators with integrated coupling capacitor.

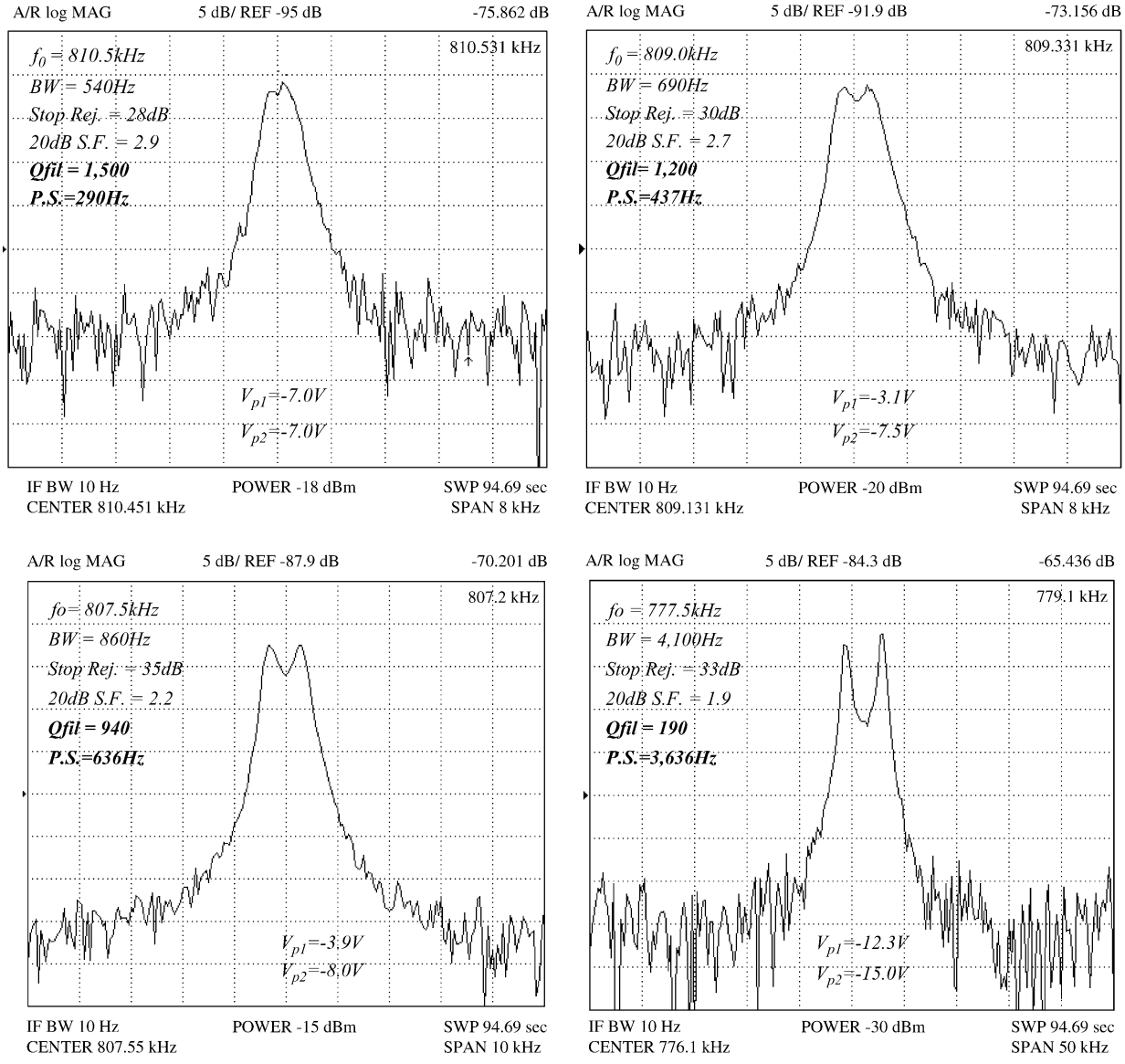

Fig. 12. Frequency response of the 800 kHz capacitively coupled filter of Fig. 10. Filter bandwidth changes by changing the applied polarization voltages. P.S.: frequency difference between the two resonance modes (peak separation) and Stop Rej.: stopband rejection.

polarization voltages, the same value of coupling capacitor results in stronger coupling (larger peak separation and larger bandwidth). Such bandwidth tunability is not possible for mechanically coupled filters and can be used for post-fabrication calibration of capacitively coupled filters. In addition to different polarities, the polarization voltages applied to the two resonators have different absolute values in order to compensate for fabrication inaccuracies and tune the center frequency of the coupled resonators to equal values.

Table 1 compares the theoretically calculated resonator parameters and filter bandwidths for different values of polarization voltages, showing good agreement between the measurement and theory. For calculation of the equivalent motional resistance of the resonators, it has been assumed that the polarization voltages are divided equally between the coupling capacitor and the resonators and the motional resistances are the values experienced by the coupling capacitor at the coupling node with $V_p = (V_{p1} + V_{p2})/2$. Deviation of the measured data from the calculated values for some of the data points is considered to be a result of uneven distribution

Table 1
Calculated resonator parameters and resonance peak separation with different polarization voltages and the measured peak separation values

V_{p1} (V)	V_{p2} (V)	R_m (MΩ)	Calculated P.S. (Hz)	Measured P.S. (Hz)
−2.2	7.0	1.84	384	290
−3.1	7.5	1.39	510	437
−3.9	8.0	1.1	643	636
−12.3	15.0	0.21	3370	3636

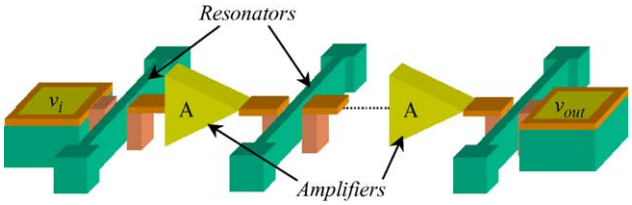

Fig. 13. Schematic diagram of an active cascaded micromechanical filter array.

of the polarization voltages between the resonators and the coupling capacitor at the coupling node due to leakage currents.

It is worth noting that in both integrated and off-chip implementation of capacitively coupled filters due to existence of comparatively large pad capacitors at the input and output nodes of the filters and large resonator equivalent impedances, it was not possible to damp the resonators and flatten the filter passband by adding terminating resistors. For the same reason, valid measurement of insertion loss could not be performed.

3. Active cascading

The alternative approach used in this work for implementation of multiple order micromechanical bandpass filters is the active cascading of resonators using active electrical components as the coupling elements (Fig. 13). In this approach, a number of resonators are cascaded with buffers or amplifiers in between to eliminate the loading effects. This results in multiplication of the transfer functions and an overall higher order transfer function for the system.

When all the stages have equal center frequencies, cascading results in order multiplication of poles, which can be interpreted as an overall higher equivalent quality factor. Mathematically, it can be shown that if n identical resonators with individual quality factors of Q_i are cascaded, the resultant Q factor of the cascade is equal to:

$$Q_{\text{total}} = \frac{Q_i}{\sqrt{10^{0.3/n} - 1}} \rightarrow Q_{\text{total}} \cong 1.2\sqrt{n}\,Q_i \quad \text{if } n \gg 1 \tag{6}$$

This concept can be used to increase the equivalent quality factor of MEMS resonators for filtering or frequency synthesis applications, in case their intrinsic Q is not high enough. In addition to Q-amplification, cascaded resonator stages provide smaller shape factor (higher selectivity). It can be shown that the shape factor of the cascaded stages is determined solely by the number of the stages regardless of the quality factor of the resonators:

$$\text{S.F.}_{40\,\text{dB}} = \sqrt{\frac{10^{4/n} - 1}{10^{0.3/n} - 1}} \rightarrow 1 \text{ as } n \text{ becomes large} \tag{7}$$

Fig. 14a illustrates simulated frequency response of cascaded resonators with different orders showing the overall Q-amplification by increasing the order of the system. Fig. 14b shows the comparison between cascaded arrays with different number of stages and identical overall Q. Despite having equal quality factors, higher order cascades provide sharper roll-off and superior selectivity (smaller shape factor).

Introducing a slight mismatch between the center frequencies of cascaded resonators results in separation of the resonance peaks and, hence, a wider bandwidth while maintaining the sidewall sharpness. However, center frequencies of cascaded devices should be close enough to avoid excessive attenuation of each stage by the other stages.

3.1. Implementation of active cascaded filters

HARPSS SCS resonators fabricated on regular silicon substrates (Fig. 7) were cascaded with JFET-input amplifiers

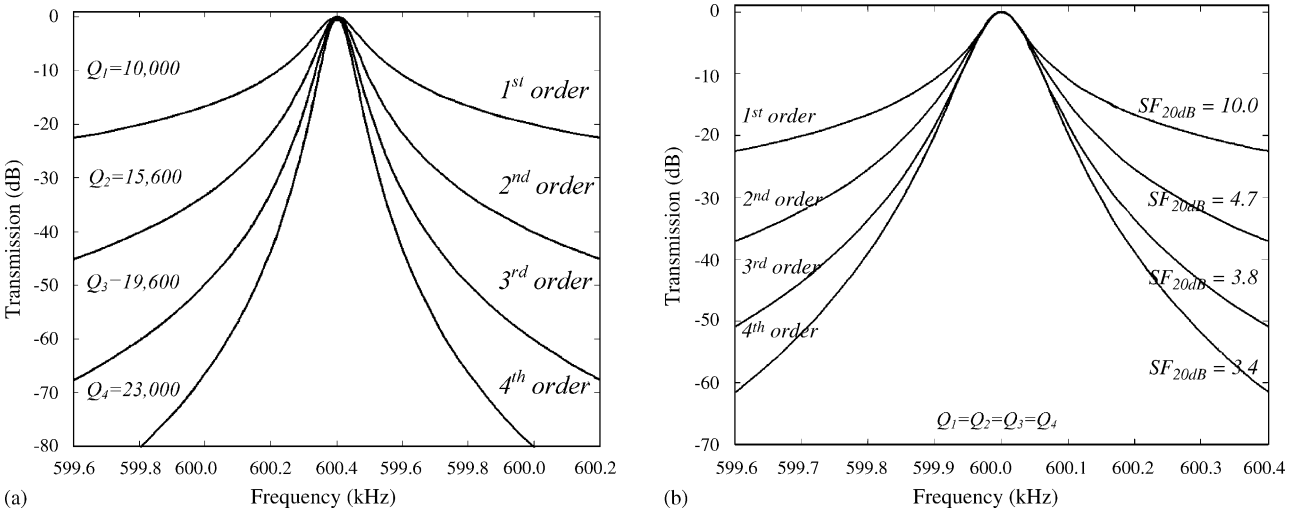

Fig. 14. Simulated frequency response of cascaded resonators with: (a) individual Q = 10,000 (600 kHz) and (b) identical overall quality factors and different orders.

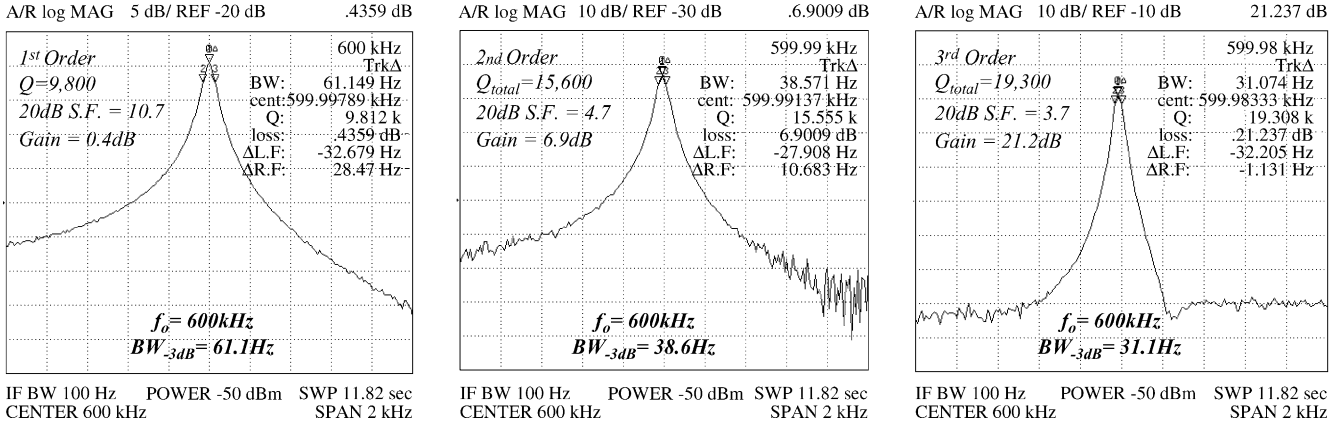

Fig. 15. Measured frequency response of cascaded resonators for achieving higher quality factors.

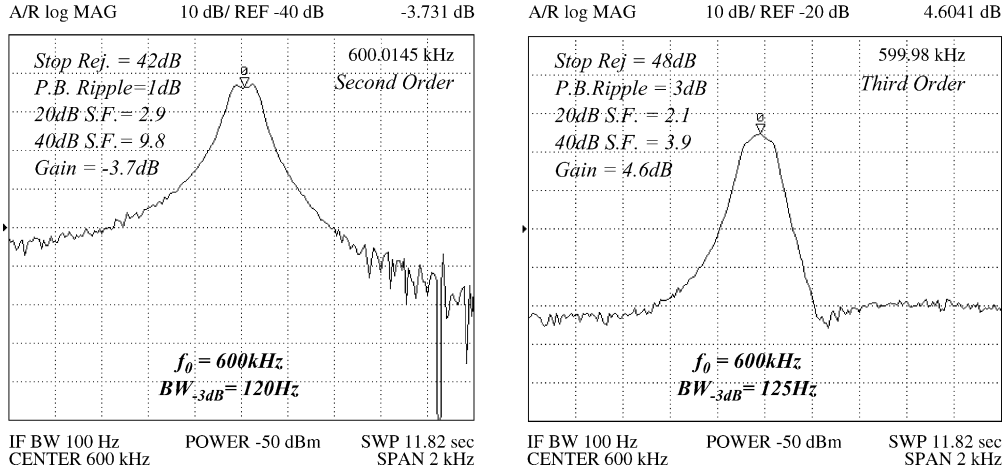

Fig. 16. Frequency response of second- and third-order bandpass filters by electrical cascading and tuning of resonators.

in between them to implement electrically cascaded filters. All the interconnections and amplifiers were off-chip.

To demonstrate Q-amplification resulting from cascading of resonators, center frequencies of the resonators were adjusted to equal values by the application of appropriate polarization voltages. Second- and third-order cascaded resonator arrays were tested under vacuum. Table 2 compares the measured and calculated overall Q values for cascaded arrays at different center frequencies, showing good agreement between the measured data and theory. Fig. 15 shows frequency response of up to three stages of cascaded resonators with equal center frequencies of 600 kHz and individual quality factors of approximately 10,000. Close to 2×, Q-amplification (Q_{overall} = 19,300) has been achieved by cascading three stages of resonators. In addition to higher Q, the cascaded stages exhibit lower shape factor (higher selectivity).

Fig. 16 shows the frequency response of the same cascaded resonator arrays when the center frequency of the resonators is tuned to slightly different values to achieve wider bandwidth filters.

Since the cascaded filters in this work are active filters, they are characterized by their gain instead of insertion loss. Gain of the filters in this case is determined by several parameters including the gain of interconnecting amplifying stages, motional resistance of the resonators and matching between the input and output of the amplifiers and resonators.

Table 2
Calculated and measured overall and individual Q's for cascaded resonators

f_0 (kHz)	Q_1	Q_2	Q_3	$Q_{\text{tot.calc}}$	$Q_{\text{tot.meas}}$
60.5	17500	16300	–	26300	28100
449	10000	18900	–	22900	23800
599	9800	10600	–	15900	15600
599	9800	10600	9000	19100	19300

4. Conclusions

Electrical-based coupling techniques for implementation of multiple order microelectromechanical resonant filters were introduced. Two different variations of electrical coupling using passive or active coupling elements were

discussed and practically demonstrated. Electromechanical modeling and operating principles of capacitively coupled resonators were described. Single crystal silicon capacitive resonators were used as building blocks for second- and third-order electrically coupled filters. Second-order capacitively coupled filters with integrated coupling capacitors and quality factors as high as 1500 were demonstrated at center frequency of 800 kHz. It was shown that the bandwidth of the capacitively coupled filters can be tuned by changing the applied polarization voltages. *Q*-amplification was demonstrated by active cascading of resonators with interconnecting amplifiers. A 2× *Q*-amplification was achieved for a three-stage cascade at 600 kHz.

Acknowledgments

This work was supported by DARPA under contract #DAAH01-01-1-R004. Authors would like to thank Reza Abdolvand for his contributions and the staff at Georgia Tech. Microelectronics Research Center for their assistance.

References

[1] R.A. Johnson, Mechnical Filters in Electronics, Wiley Interscience, 1983.
[2] K. Wang, et al., High-order medium frequency micromechanical electronic filters, JMEMS 8 (4) (1999) 534.
[3] A.-C. Wong, et al., Anneal-activated, tunable, 68 MHz micromechanical filters, Sens. Actuators 99 (1999) 1390–1393.
[4] L. Lin, et al., Microelectromechanical filters for signal processing, JMEMS 7 (3) (1998) 286.
[5] D.S. Greywall, et al., Coupled micromechanical drumhead resonators with practical applications as electromechanical bandpass filters, J. Micromech. Microeng. 12 (2002) 925–938.
[6] K. Wang, et al., IEEE Ultrasonics Symposium, Q-Enhancement of Microelectromechanical Filters via Low Velocity Spring Coupling, 1997, pp. 323–327.
[7] S. Pourkamali et al., A 600 kHz electrically coupled MEMS bandpass filter, MEMS'03, 2003, pp. 702–705.
[8] S.Y. No, et al., Single crystal silicon HARPSS capacitive resonators with submicron gap spacings proceedings, Hilton Head, 2002, pp. 281–284.
[9] F. Ayazi, K. Najafi, High aspect-ratio combined poly and single-crystal silicon (HARPSS) MEMS technology, JMEMS 9 (3) (2000) 288–294.
[10] S. Pourkamali, F. Ayazi, Fully single crystal silicon resonators with deep-submicron dry-etched transducer gaps, MEMS'04, 2004, pp. 813–816.
[11] D. Galayko, et al., Microelectromechanical variable-bandwidth IF frequency filters with tunable electrostatical coupling spring, MEMS'03, 2003, pp. 153–156.

Biographies

Siavash Pourkamali received BS degree in electrical engineering from Sharif University of Technology, Iran, in 2001 and MS degree from Georgia Institute of Technology, Atlanta, in 2004. Currently, he is pursuing PhD degree in Electrical Engineering Department, Georgia Institute of Technology. His main research interests are in the areas of rf MEMS resonators and filters, silicon micromachining technologies and integrated microsystems. He is a 2005 recipient of the Sigma Xi best MS thesis award.

Farrokh Ayazi was born in February19, 1972. He received BS degree in electrical engineering from the University of Tehran, Iran, in 1994 and MS and PhD degrees in electrical engineering from the University of Michigan, Ann Arbor, in 1997 and 2000, respectively. He joined the faculty of Georgia Institute of Technology in December 1999, where he is currently an assistant professor in the School of Electrical and Computer Engineering. His current research interests are in the areas of low and high frequency micro- and nanoelectromechanical resonators, VLSI analog integrated circuits, MEMS inertial sensors and microfabrication technologies. He is a 2004 recipient of the NSF CAREER award, the 2004 Richard M. Bass Outstanding Teacher Award and the Georgia Tech. College of Engineering Cutting Edge Research Award for 2001–2002. He received a Rackham Predoctoral Fellowship from the University of Michigan for 1998–1999.